RESEARCH ARTICLE

Enhancement of Vehicular Visible Light Communication Using Spherical Detector and Custom Lens Combinations

SELMA YAHIA[1], **YASSINE MERAIHI**[1], **AMAR RAMDANE-CHERIF**[2], **TU DAC HO**[3], **(Member, IEEE), AND HOSSIEN B. ELDEEB**[4], **(Senior Member, IEEE)**

[1]LIST Laboratory, University of M'Hamed Bougara Boumerdes, Boumerdes 35000, Algeria
[2]LISV Laboratory, University of Versailles Saint-Quentin-en-Yvelines, 78140 Velizy, France
[3]Department of Electrical Engineering, UiT The Arctic University of Norway, 8514 Narvik, Norway
[4]Center for Cyber-Physical Systems, Department of Electrical Engineering and Computer Science, Khalifa University, Abu Dhabi, United Arab Emirates

Corresponding author: Tu Dac Ho (tu.d.ho@uit.no)

ABSTRACT Vehicular Visible light communication (VLC) technology has recently attracted much interest from researchers and scientists. This technology enables connectivity between vehicles and infrastructures along the road by using vehicles' headlights and taillights as wireless transmitters. The reliability of vehicle-to-vehicle (V2V) VLC systems is affected by several factors, such as car mobility, optics system design, and visibility conditions, where the first two have the most impact on the VLC system performance. This paper, therefore, focuses on the relative positions of the cars and the design of the optics, especially on the receiving end, which has been proposed with the use of a polar detector instead of the rectangular detectors commonly used in the literature. We investigate the achievable gain compared to the conventional detector for different vehicle locations, utilizing a professional optical system design and ray tracing approach. Then, to improve the performance, we introduce the utilization of an imaging receiver by integrating the polar detector with different optical commercial lens combinations, such as Fresnel and Aspherical lenses. To further improve the V2V system performance, we propose a novel optical lens combination design by integrating double-convex lens with half-Plano-concave lens, which allows the correction of more optical aberrations, such as chromatic and spherical aberration. Utilizing the non-sequential ray tracing tools, we designed these VLC systems and perform a realistic channel modeling study considering the typical 3D CAD models of vehicles and roads as well as the possibility of horizontal and vertical movement between the vehicles. Based on the channel impulse responses (CIRs) obtained from the ray tracing simulations, we analyzed the performance of V2V VLC systems with all lens combinations at different vehicle positions on the road. We further investigated the impact of different system parameters on the overall V2V system performance, such as receiver diameter and bandwidth. The obtained results demonstrated that with a carefully chosen system and lens parameters, the proposed system design of lens combination provides an enhancement of up to 7 dB in total received power compared to the case without a lens. Our results also revealed that the proposed system design outperforms the benchmark ones for all lateral displacements and longitudinal distances.

INDEX TERMS Vehicular communications, visible light communication, optical lens combination, polar detectors.

I. INTRODUCTION

Vehicular communication plays a critical role in improving road safety, realizing autonomous driving, and offering comfortable driving to road users. It enables wireless connectivity between cars, roadside units, pedestrians and passengers [1]. In addition to the radio frequency (RF)-based technology, visible light communication (VLC) technology was proposed as an alternative and complementary solution using light-emitting-diodes (LEDs) as transmitters

The associate editor coordinating the review of this manuscript and approving it for publication was Barbara Masini.

and photodetectors (PDs) as receivers. VLC can be used in vehicular communication networks enabling Vehicle-to-Vehicle (V2V) and/or Vehicle-to-Infrastructure (V2I) communications [2].

Vehicular VLC (VVLC) technology can benefit from high throughput directional links between vehicles and infrastructure (e.g. uplink and downlink between vehicles and roadsides). In fact, safety messages can be sent from road infrastructures to approaching vehicles (using traffic lights and streetlights as transmitters), as well as from vehicles to vehicles (using headlights and/or taillights as transmitters) [3]. Furthermore, Vehicles can share data about their status (e.g. speed, position, acceleration, etc.), which increases vehicle awareness. Besides safety, VVLC can be utilized to enhance the efficiency of the transportation system by offering location-based services and optimal alternative routes.

However, the vehicular environment has specific properties that differ from other scenarios and has a direct influence on the performance of the vehicular system. In particular, adverse weather conditions can severely degrade the performance of the VVLC system. Many research activities have been conducted in this area [4], [5], [6]. Furthermore, the light received in a vehicular system is exposed to different parasite lights, including sunlight, ambient illumination, and light signals from multiple LEDs, leading to some problems, such as output saturation and interference. A couple of studies have reported solutions to these issues, as in [7], [8], and [9]. Mobility is another challenge for the VVLC system due to its line-of-sight (LoS) requirement. Most recent research in the literature has been conducted in static conditions where the transmitter and receiver are in a straight line [10], [11], [12]. However, in real applications, the angle of the incident light and the distance between the transmitter and the receiver are usually variables. An effort to address this issue using multiple PDs is presented in [13] and [14]. For instance, in the work of Cui et al. [13], three PDs were used, and the one with the highest received power was selected. Also, in [14] four PDs were deployed to prevent interruptions in a V2V-VLC system when changing lanes on a two-lane road. Nevertheless, they cannot cover all directions, and the receiver still has a limited view. To overcome these limitations, a non-imaging angle diversity receiver [15], [16] was proposed as a potential solution. It consists of different detection branches, each with its own optical detector, orientated at specific angles, allowing reception from various angles. However, the work of [17] shows that the non-imaging optical systems are relatively limited while the imaging receivers potentially offer better performance. The latter consists of an array of PDs and a lens to collect and focus the light rays from a wide angle to a small receiving area.
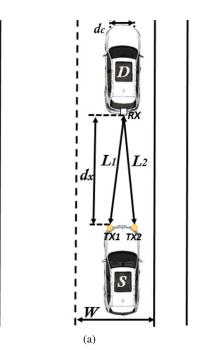
This can ensure a large collection of lights and hence improve performance. Generally, different kinds of lenses can be used, i.e. hemispherical, convex, and fisheye lenses. The imaging receiver is considered a viable option to mitigate the impact of inter-symbol interference (ISI) and ensure the
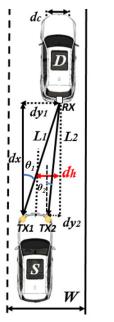
mobility of the VLC system. It was applied for the first time in indoor environments to improve the performance of the Multiple-Input Multiple-Output (MIMO) VLC system and reduce the channel correlation [18], [19], [20], [21], [22], [23], [24]. For example, the authors in [18] utilized a convex lens-based imaging receiver in a MIMO system with spatial multiplexing (SMP) transmission scheme. The results demonstrated that a significant performance improvement could be achieved with an imaging receiver compared to a non-imaging receiver. This is because the system with a non-imaging receiver is strongly affected by spatial correlation and spatial interference while using an imaging receiver can effectively combat these interferences and maximize the received power. The authors in [20], [21], and [22] presented a hemispherical lens-based imaging receiver that has a wider field of view (FoV) and can separate the signal from various LEDs. Also, an imaging receiver scheme based on a fisheye lens was proposed in [23] and [24]. It could achieve omnidirectional reception with ultra-wide FoV, compact size, and high image quality. However, the applications of the imaging receiver in outdoor scenarios are relatively new, and therefore, further efforts are required to investigate its performance. For instance, the authors in [25], applied a hemispherical lens to improve the performance of a vehicular MIMO-VLC system. Similarly, in the work of Yoo et al. [26], a conventional lens is applied to minimize the noise interference spectrum of sunlight in a V2V-VLC system. Also, in [27], the authors experimentally investigated the effect of the combination of convex lens on a V2V-VLC system. The results in that work demonstrated that utilizing the lens can also improve the performance in an outdoor environment. All previous studies [25], [26], [27], however, have considered the usage of a single PD, one lens type, and the case of perfect alignment, where the two cars are travelling in the same lane without any lateral shift, which does not reflect reality.

In this paper, we investigate the performance of the V2V-VLC system using an imaging receiver with different kinds of optical lenses, including Fresnel, Aspherical, and combined lenses. We further propose the use of a polar detector (which has not been reported in the literature) instead of multiple PDs to collect rays from many directions. We perform a channel modeling study based on the non-sequential ray-tracing approach in OpticStudio®, which was validated in [4]. We first quantify the total received power for the different assumed scenarios considering the asymmetrical radiation pattern of the headlights same as the possibility of both the horizontal and the vertical displacement between the vehicles. We further address the effect of receiver type, lateral shift, receiver diameter, and bandwidth on the performance of the considered systems. Then, the packet delivery ratio for different lateral shifts is also investigated.

The remainder of this paper is organized as follows. In section II, we describe our system model, the different steps of our channel modeling approach, and the design of the optical system model. In section III, we give the performance
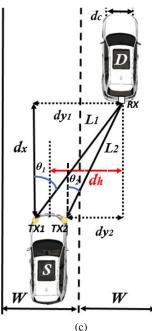
(a)   (b)   (c)

FIGURE 1. V2V-VLC scenarios under consideration.

metrics. Section IV presents the simulation results and discussion. Finally, we conclude in Section V.

II. V2V-VLC SYSTEM AND CHANNEL MODEL
In this section, we explain the system model, the different steps of our channel modeling approach, and the design of the optical system model.

A. SYSTEM MODEL
As illustrated in Fig. 1, we consider a V2V-VLC system in a two-lane road with a lane width of W. The source vehicle S communicates with the destination vehicle D through its headlamps (denoted by TX1 and TX2) which are separated horizontally by a distance d_c from each other. These car headlights transmit information to the destination vehicle (i.e., D) with an optical power P_t. It should be noted that, unlike the interior LEDs, the vehicle's headlamps have an asymmetrical intensity pattern that is supposed to provide full illumination from the front and sides while minimizing glare to oncoming vehicles and other road users. As an example, Fig. 2 shows different cross-sections to illustrate the headlamp's asymmetrical intensity pattern. The blue curve shows the headlight intensity distribution when looking from the side, while the green curve shows the same pattern when looking down from above.

On the other hand, vehicle D is equipped with an imaging receiver (PDs and lenses) to focus the light, mounted at its back, at the same height as the headlamps. Generally, one or multiple PDs, installed on the back of the destination car are used as wireless receivers. As a more alternative to conventional PDs, the polar detector with a radius of r and a responsivity of R can be employed. The polar detector is a
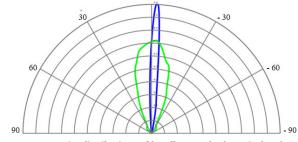

FIGURE 2. Intensity distributions of headlamp at both vertical and horizontal planes.

spherical-shaped detector that displays radiant intensity data on a polar graph (see Fig. 3). Its polar angle ranges from 1 to 180 degrees in each cross-section (which forms a complete sphere) [28], ensuring a large collection of rays from different directions. Thus, it will be more convenient for the mobility of vehicles. We further define d_x and d_h, which represent the vertical and the horizontal distance between S and D.

B. CHANNEL MODEL
In this paper, we adopt the non-sequential ray-tracing channel modeling approach of OpticStudio® simulator. This technique enables rays to spread in any order through the environment, allowing them to split, scatter and reflect on the surrounding objects. It was initially adopted to model the indoor [29], [30], [31] and underwater [32], [33] VLC channel, and then applied for outdoor VLC channel [3]. The main steps of this simulator can be illustrated as follows:

1) STEP 1: 3D MODEL DESIGN
Firstly, the 3D simulation environment of the considered V2V-VLC system is built in the OpticStudio® simulator
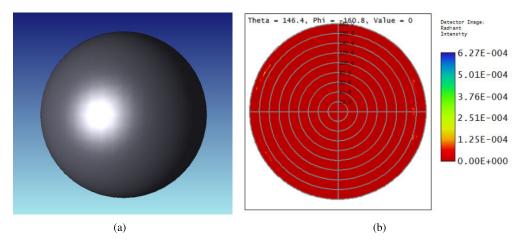
FIGURE 3. (a) 3D polar detector (b) Radiant intensity data.

platform, where the CAD models of the road and vehicles are designed and imported into the environment. These CAD models are specified by their criteria, such as surface coating and reflection and scattering proprieties utilizing the "Coating material" tool.

2) STEP 2: DATA SPECIFICATIONS
In this step, the specifications of the optical transceiver, including the source (the number of emission rays, the radiation pattern, spectral intensity, the optical strength, and orientations) and receiver (aperture diameter, field of view, active region) characteristics are added as input parameters using "Source Type" tool.

3) STEP 3: NON-SEQUENTIAL RAY-TRACING PROCESSING
Once the simulation scenario is established, the non-sequential ray-tracing model is performed to generate an output file containing path length and received power information for each ray generated by the light source and absorbed by the detector. These statistics are then imported into Matlab for further processing. Thus, the received power at the detector can be given by [34]

$$Pr = P_t \times G_L \int_0^\infty h(t)dt, \qquad (1)$$

where P_t is the transmitted power, G_L is the gain of the optical lens, and $h(t)$ is the channel impulse responses (CIRs) that can be given by

$$h(t) = \sum_{i=1}^{2} \left(\sum_{k=1}^{M} P_{i,k} \delta \left(t - \tau_{i,k} \right) \right), \qquad (2)$$

where $\tau_{i,k}$ and $P_{i,k}$ denote respectively the propagation delay and the power of the kth ray, $k = 1, .., M$, transmitted from the ith transmitter and received by the PD. Also, δ is the Dirac delta function.

Recently, the authors in [34] proposed a channel gain model for a single detector, which is given by the following equation

$$H_C = \int_0^\infty h(t)dt = \frac{1}{2} \sum_{i=1}^{2} \left(\frac{D_R \left(d_x/L_i \right)^{1/\varepsilon}}{\zeta L_i} \right)^2, \qquad (3)$$

where D_R is the receiver diameter, ε and ζ are correction coefficients, and Li denotes the transmission distance between the ith transmitter and the receiver. It can be given by $Li = \sqrt{d_x^2 + d_{y_i}^2}$, where $d_{y_i} = d_h \pm d_c/2$.

In (1), G_L is the optical lens gain which is related to the different types of lenses used in the system. In the next section, we explain the different types of lenses considered in our system.

C. OPTICAL SYSTEM DESIGN
For optical system design, we use the Zemax OpticStudio® 21.2 software to introduce three lenses design. The utilized optic design includes Fresnel, Aspherical, and the proposed design, a combination of double-convex with half Plano concave lenses, each with its own diameter Dr and focal length f_l. These optics are placed in front of the PD to concentrate the incident light on the sensitive area of the PD. In the following, we present the principle of each of these considered lenses.

1) FRESNEL LENS
Fresnel lens consists of a planar surface on one side and a series of concentric grooves replicated in the plastic on the other side (see Fig. 4(a)). These contours are designed to provide a variable deviation angle on the lens surface, bending parallel light rays to a common focal length f_l [35]. Fresnel lenses offer good optical performance at an affordable price, with reduced weight and thickness. Their use in receiver stages has been described in previous work, reporting achievable distances of several meters at 1 kbps in a laboratory prototype [5]. They have also been applied in indoor VLC scenarios, as in [36]. The portion of the light reflected (Fresnel reflection) from the surface of an ordinary dielectric

material (such as glass) is given by [37]:

$$R = \frac{1}{2}\left[\frac{\sin^2(\theta - \theta')}{\sin^2(\theta + \theta')} + \frac{\tan^2(\theta - \theta')}{\tan^2(\theta + \theta')}\right], \quad (4)$$

where θ and θ' are the angles of incidence and refraction, respectively.

2) ASPHERICAL CONDENSER LENS

Unlike the traditional lens with a spherical surface, the Aspherical lens has a more complex surface whose curvature gradually changes from the lens's center to its edge. It can be used to focus collimated light (condensation) into a single image element with a short focal length. This lens has an aspheric surface on one side and a Plano surface on the other side, as shown in Fig. 4(b). The shape of this lens allows for reducing the spherical aberration considerably, even for very low f-numbers. This lens is mainly used in condenser or lighting applications. It is also used when high light gathering power is required, for example, for focusing on detectors or fibers.

For a lens with curvature radius of r and refractive index of n, the focal length can be given by [38]:

$$f_l = \frac{r}{n-1}. \quad (5)$$

For the non-negligible thickness of the lens, we introduce the distance between the flat surface of the lens and the focal plane of the image, called back focal length (B_f) (see Fig. 4(b)). It can be given as follows:

$$B_f = f_l\left[1 - \frac{t_c(n-1)}{n \times r}\right], \quad (6)$$

where t_c is the center thickness.

3) COMBINED LENS

In contrast to a simple lens, a compound lens is a set of single lenses with a common axis. In our system, we proposed a combination of two lenses kept in contact with each other: the double-convex and the half-Plano-concave (see Fig. 4(c)). Using these multiple lenses allows the correction of more optical aberrations, such as chromatic and spherical aberration. The common focal length f for the resulting optic can be given by [39]:

$$\frac{1}{f_l} = \frac{1}{f1} + \frac{1}{f2}, \quad (7)$$

where $f1$ and $f2$ are the focal lengths of the first and second lenses, respectively.

III. PERFORMANCE METRICS

In this section, we analyze the performance of our proposed V2V-VLC model by considering the Packet error rate (PER) as performance metric, which is given by [40]:

$$\text{PER} = 1 - (1 - P_e)^n, \quad (8)$$

where n denotes for the packet length and P_e is the end-to-end BER. For M-ary Pulse-Amplitude Modulation (PAM), P_e is given by [41, Chapter 3]

$$P_e = \frac{(M-1)}{M \log_2(M)} \text{erfc}\left(\sqrt{\frac{3}{2(M-1)(2M-1)}\gamma}\right), \quad (9)$$

where $\text{erfc}(x) = \frac{2}{\sqrt{\pi}}\int_x^\infty e^{-t^2}dt$, M is the modulation order, and γ is the signal-to-noise-ratio (SNR), which takes the form of

$$\gamma = \frac{R^2(P_t H)^2}{\sigma_t^2}, \quad (10)$$

where, R denotes the PD responsivity, σ_t^2 is the noise variance, and $H = H_C \times G_L$ is the total channel gain between the car and the receiver. It contains the channel loss H_C (i.e. due to the geometry of transceivers and the propagation through free space), which is given by (3) and the gain of the optical lens system (G_L), which depends on the utilized lens system and the incident angle. Thus, by replacing (3) in (10), γ is written as follows:

$$\gamma = \frac{R^2\left(\frac{1}{2}P_t G_L \sum_{i=1}^2 \left(\frac{D_R\left(d_x/\sqrt{d_x^2 + d_{y_i}^2}\right)^{1/\varepsilon}}{\zeta\sqrt{d_x^2 + d_{y_i}^2}}\right)^2\right)^2}{\sigma_t^2}. \quad (11)$$

From (11), the final expression of PER is given by (12), as shown at the bottom of the next page.

IV. SIMULATION RESULTS AND DISCUSSION

A. SCENARIOS UNDER CONSIDERATION

As shown in Fig. 1, we consider a V2V scenario in a two-lane road, where the source vehicle S communicates with the destination vehicle D, assuming different positions on the road. Specifically, we consider three scenarios:

- **Scenario 1:** We assume that S and D are placed in the center of the same lane and moving in a straight line, where d_h= 0 m (see Fig. 1(a)).
- **Scenario 2:** We assume that S and D are moving in the same lane, but there is a misalignment between them which results in a horizontal shift of d_h (see Fig. 1(b)).
- **Scenario 3:** We assume that S and D move in adjacent lanes, forming a horizontal offset of d_h (see Fig. 1(c)).

Furthermore, we investigate the V2V-VLC system with different receiver types. We assumed to use three configurations with single PD, multiple PDs (three in this investigation), and a polar detector.

B. SIMULATION PARAMETERS

In this section, we present the numerical results of the V2V-VLC system with the presence of an imaging receiver. We consider a two-lane road with a lane width of $W = 4$ m [42]. The road type R2 consisting of 60% gravel larger than 10 mm as defined in [43] is considered. We use a vehicle modeled as a black CAD object with the dimensions of the

FIGURE 4. (a) Fresnel Lens (b) Aspherical Condenser Lens (c) Combination of Double-convex with Half Plano-concave.

TABLE 1. Main simulation parameters for V2V system.

System parameters	Values
Road Parameters	
Type	R2 [43]
Material	Asphalt
Lane width	4 m [42]
Transmitter Parameters	
Light wavelength	400 nm-700 nm
Power, P_t	1 W
Optics Parameters	
Diameter, Dr, for L1, L3 lenses, respectively.	50 mm, 50 mm
Dimension for L2	63.5×63.5 mm
Focal length, f_l, for L1, L2, L3 lenses, respectively	35.7 mm, 50.8 mm, 68.6 mm
Receiver Parameters	
Radius, r	10 mm, 15 mm, and 20 mm
Noise parameters	
Bandwidth, B	5 MHz
Spectral density, N_0	$10^{-21} A^2/Hz$

Audi A8 model [44]. We assume clear weather, $P_t = 1W$ and $d_h = 0$ m, 1 m, 2 m, 3 m, and 4 m. At the receiver side, we assume the usage of three receiving types: a single detector with a responsivity of $R = 0.54$ A/W, three PDs, and a polar detector with a radius of $r = 10$ mm, 15 mm, and 20 mm. They are placed at the back of vehicle D at a high of 700 mm. Besides, we utilize three optics placed above the imaging plane. Specifically, we employ three lenses system:

- **L1:** We use a commercial Aspheric Condenser Lens [45] with a $Dr = 50$ mm, an index of refraction of $n = 1.49$, and $f_l = 35.7$ mm.
- **L2:** We use a commercial Fresnel lens [46] with a dimension of 63.5×63.5 mm, and a $f_l = 50.80$ mm.
- **L3:** We use a combined lens with a $Dr = 50$ mm, and $f_l = 68.6$ mm.

C. RESULTS AND DISCUSSION

In the following, we first present the received power as a function of distance when considering different receiver diameters, lateral offsets, and lens system designs for all scenarios. Then, the PER versus the distance for different lateral shifts and bandwidths is also investigated.

1) RECEIVED POWER VERSUS DISTANCES

In Fig. 5, we present the received power versus distance for different lateral shifts, $d_h = 0, 1, 2, 3$, and 4 m. we assumed to use these three different configurations with single PD, multiple PDs (three in this investigation), and a polar detector. Having features of a wide coverage area which enables a better collection of rays from all directions, the optics performance of the polar detector can be better than that for the single and multiple PDs cases. For example, at $d_h = 0$ and $d_x = 15$ m, the total received power is -44 dB for the case of the polar detector. This reduces to -49 dB and -54 dB for the three and single PD cases, respectively. It is also observed from Fig. 5 that the lateral shift severely affects the received power, particularly at shorter distances. For example, consider the case of a polar detector and $d_x = 10$ m, the total received power is -41 dB for $d_h = 0$. This reduces to -41.6 dB, -43.5 dB, -46.5 dB, and -50 dB for $d_h = 1$ m, $d_h = 2$ m, $d_h = 3$ m, and $d_h = 4$ m, respectively. When the distance becomes significantly large, the effect of lateral offset decreases. This is due to the fact that the angle of arrival at the receiver decreases as the inter-vehicle distance increases, allowing more power to be collected. For example, consider $d_x = 50$ m and polar detector case, the total received powers are given as -53.6 dB, -53.8 dB, -53.9 dB, -54 dB, and -53.9 dB for $d_h = 0$ m, $d_h = 1$ m, $d_h = 2$ m, $d_h = 3$ m, and $d_h = 4$ m, respectively.

Figure 6(a) shows the received power as a function of distance, assuming different polar detector radius

$$\text{PER} = 1 - \left(1 - \left(\frac{(M-1)}{M \log_2(M)} \text{erfc}\left(\sqrt{\frac{3}{2(M-1)(2M-1)}\left(\frac{R^2\left(\frac{1}{2}P_t G_L \sum_{i=1}^{2}\left(\frac{D_R\left(d_x/\sqrt{d_x^2+d_{y_i}^2}\right)^{1/\varepsilon}}{\zeta\sqrt{d_x^2+d_{y_i}^2}}\right)^2\right)^2}{\sigma_t^2}\right)}\right)\right)\right)^n . \quad (12)$$
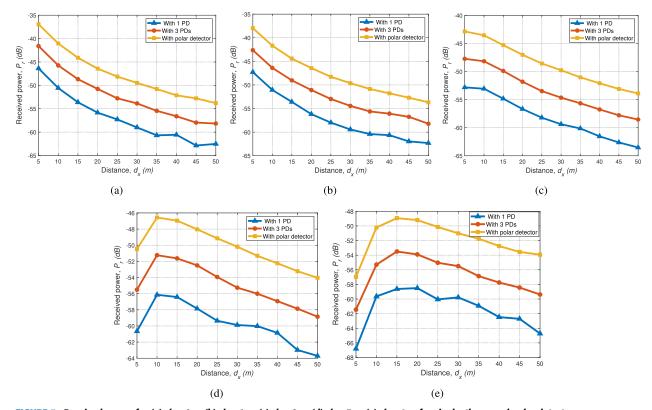
FIGURE 5. Received power for (a) d_h = 0 m (b) d_h = 1 m (c) d_h = 2 m (d) d_h = 3 m (e) d_h = 4 m for single, three, and polar detectors.
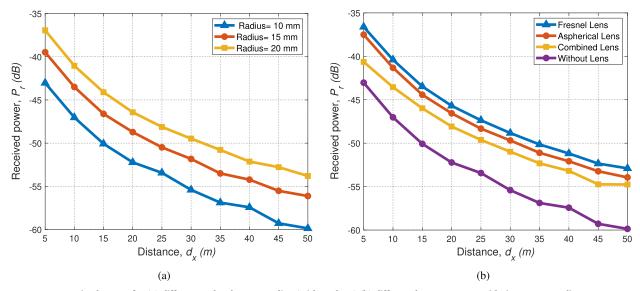

FIGURE 6. Received power for (a) different polar detector radius (without lens) (b) different lens system considering 10 mm radius.

(i.e., $r = 10$ mm, $r = 15$ mm, and $r = 20$ mm). We consider that the two cars are perfectly aligned ($d_h = 0$ m) and no lenses are used. It is observed that the total received power increases with the increase of the radius of the polar detector. This is due to the fact that increasing the radius increases the diameter of the detector, which in turn increases the overall detector collection area. Thus, for an increased detector area, the maximum light intensity captured by the receiver

increases. This is expected because the intensity captured by the receiver is proportional to its collection area. For example, consider $d_x = 10$ m, the total received power is -47 dB. This claims to -43 dB and -41 dB for $r = 15$ mm and $r = 20$ mm, respectively.

In the following, we evaluate the effect of lens usage on the performance of the V2V system under consideration. Toward this, we compare a V2V-VLC system without a lens
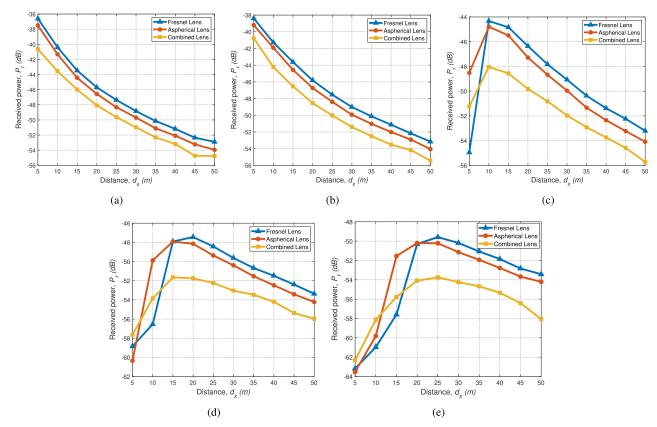
FIGURE 7. Received power for (a) d_h= 0 m (b) d_h= 1 m (c) d_h= 2 m (d) d_h= 3 m (e) d_h= 4 m for a polar detector with a radius of 10 mm.

and the ones with different types of lenses (i.e., Fresnel lens, Aspherical Lens, and combined lens). To make a one-to-one comparison, we assume the following assumptions for all scenarios: $r = 10$ mm, $d_h = 0$ m, and the usage of a polar detector.

Fig. 6(b) presents the total received power versus distance for all lens design cases. It is observed that the addition of optics in the considered system can improve the performance for both short and long distances. This is due to the ability of the lenses to collect rays from different directions that the detector cannot reach (which means increasing the number of collected rays) and focusing them on the PD sensitivity area. For example, consider $d_x = 15$ m and the case of the L2 lens. An improvement of 7 dB of the received power is obtained compared to the case without a lens. Similarly, improvements of 6 dB and 4 dB are recorded at a distance of $d_x = 10$ m, using the L1 and L3 lenses, respectively, compared to the case without lens.

In the following, we investigate the effect of the lateral shift on the received power for all lens systems under consideration, assuming a radius of $r = 10$ mm.

In Figure 7(a), we present the received power versus distances for different lens systems. We assume that the two cars are perfectly aligned (i.e., $d_h = 0$ m). It is observed that the L2 lens gives good performances for all distances. This is because the L2 lens focuses the rays from the emitter into a single focus, better than the L3 and L1 lenses where the

incoming light rays converge at different focal points due to spherical aberration along the optical axis (see Fig. 4). For example, consider $d_x = 10$ m and $r = 10$ m, the total received power is recorded as -40 dB using L2 lens. It reduces to -41.3 dB and -43.3 dB for L1 and L3 lenses, respectively.

In Figure 7(b), we consider the case of misalignment where $d_h = 1$ m. It is clear that the L2 lens still gives the best results for all distances, resulting in a good performance with an improvement of 1 dB and 3 dB at a distance of $d_x = 20$ m compared to the case with L1 and L3 lenses, respectively.

Figure 7(c) indicates the total received power versus distance assuming $d_h = 2$ m. It is observed that for short distances from 5 m to 9 m, the L1 lens gives good results compared to the other types of lenses (i.e., L2 and L3). Beyond this distance, the L2 lens becomes the best. This behavior is explained by the fact that at short distances and misalignment cases, the incidence angle of transmitted rays is large and the L1 lens has a wide angle of view (from 1 to 180°) that is oriented in all directions in contrast to the L2 lens that has a small angle of view. This allows the L1 lens to capture more rays than the L2 lens and the L3 lenses. On the other hand, at long distances, the angle of incidence is reduced, and therefore the L2 lens gives the best performance. For instance, consider a short distance of $d_x = 8$ m, the received power is 47 dB for the case of L1 lens. This reduces to -49 dB and -50 dB for L2 and L3 lens cases. Also, consider $d_x = 30$ m, the total received power is -49 dB for the
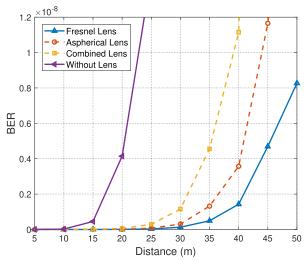
FIGURE 8. BER versus distance for different lens cases.

FIGURE 9. PER versus distance for all considered scenarios.

L2 lens, which reduces to -50 dB and -52 dB for L1 and L3 lenses. In Figure 7(d), we present the received power versus distance, considering $d_h = 3$ m. It is observed that the best performances are obtained using the L3 lens at a short distance of $d_x = 5$ m. After that, the L1 lens becomes the best for a range of distance from 6 m to 15 m. Beyond this distance, the L2 is the best. For example, consider $d_x = 5$ m, the total received power is -57 dB, -58, and -60 dB for L3, L2, and L1 lenses. Also, consider $d_x = 10$ m, the received power becomes -50 dB, -54 dB, and -57 dB for L1, L3, and L2 lenses case, respectively. In addition, consider $d_x = 25$ m, the received power is given as -48 dB, -49 dB, and -52 for L2, L1, and L3 lenses, respectively.

Figure 7(e) shows the received power versus distance, assuming $d_h = 4$ m. It is observed that for short distances from 5 m to 10 m, the L3 lens gives the best performance. While for the ranges d_x of 11 m to 20 m, the L1 lens offers the best performance. Beyond that, the L2 lens is the best. In particular, received powers of -58 dB, -59 dB, and -60 dB are obtained at $d_x = 10$ m using L3, L1, and L2 lenses, respectively. Also, consider $d_x = 15$ m and the cases of L1, L3, and L2 lenses, the total received powers are -51.5 dB, -55.7 dB, and -57.5 dB, respectively. Finally, for $d_x = 30$ m, the received powers are -50 dB, -51 dB, and -54 dB using L2, L1, and L3 lenses, respectively.

To further validate the obtained simulation results in our work, we have compared the BER performance metric with existing literature research at varying inter-vehicle distances. Without loss of generality, consider distances of 15 m, 20 m, and 25 m as examples, and not using the lens (only a single PD), the BERs obtained from [47] were 4.5×10^{-7}, 5×10^{-7}, and 8×10^{-5}, respectively. However, in our paper, when implementing a polar detector at the receiving side, BERs of 0.05×10^{-8}, 0.4×10^{-8}, and 1.4×10^{-8} were obtained (See Fig. 8), at the same example distances, respectively. This improvement has denoted the advantage of the polar detector over the single photodetector in [47] (see Fig. 5). Similarly,
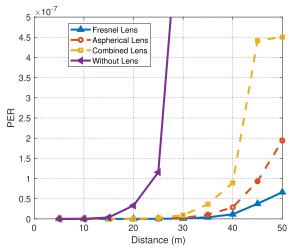
we continue to compare performances in a more complicated scenario, where [47] implemented a conventional lens and our study implemented a combined lens. The results are as follows, BERs in our research has significantly improved, reduced from 10^{-7}, 1.01×10^{-7}, and 1.02×10^{-7} (obtained from [47]) and down to 0.6×10^{-11}, 0.55×10^{-10}, and 2.8×10^{-10} for distances of 15 m, 20 m, and 25 m, respectively. Also, the authors of [26] and [48] use a conventional lens and BERs of 8×10^{-7}, 7×10^{-5}, and 9×10^{-5} are recorded at distances 15 m, 20 m, and 25 m, respectively, in [26], while [48] achieved BERs of 10^{-7}, 10^{-7}, and 10^{-7} at the same distances. This decreases to 0.7×10^{-11}, 5.9×10^{-11}, and 2.9×10^{-10} in our work using the proposed combination lens (see Fig. 8).
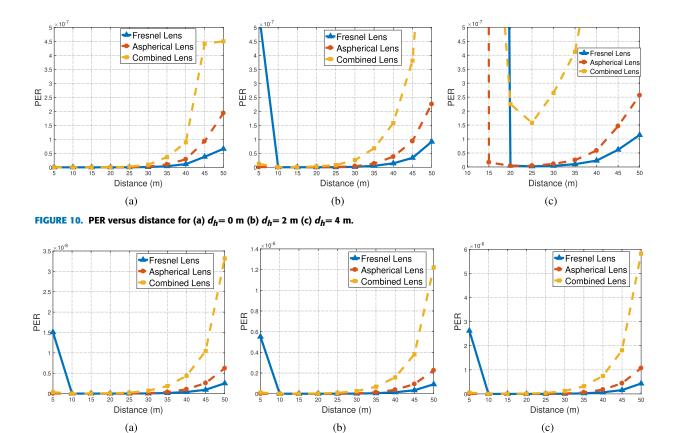
2) PACKET ERROR RATIO VERSUS DISTANCE

In this section, we investigate the PER performance of all considered scenarios. Fig. 9 presents the PER versus distance for all scenarios under consideration. We consider $d_h = 0$ m and $r = 10$ mm. It is clear that error-free communication is remarkably achieved up to 15 m for the case without a lens. While in the lens case, a remarkable error-free communication is achieved up to 30 m with an improvement of 15 m compared to the case without lens. Beyond that, degradation of performance is also observed. For example, consider $d_x = 25$ m, the PER is set to 1.5×10^{-7} for the case without a lens. In contrast, it refers to zero for all considered lens systems.

In the following, we address the effect of lateral shift (i.e., $d_h = 0$ m, $d_h = 2$ m, and $d_h = 4$ m) on the performance of the V2V VLC systems under consideration.

In Fig. 10, we present the PER versus distance for different lens systems, considering different lateral offsets. We assume $d_h = 0$ m, 2 m, and 4 m. It is observed from Fig. 10(a) (i.e., $d_h = 0$ m) that error-free communication is remarkably achieved up to 30 m with all lenses. Beyond that, a degradation in performance is observed up to 50 m, where the L2 lens shows the best performance compared to other lens systems. For example, consider $d_x = 20$ m, the PER refers to zero for

FIGURE 10. PER versus distance for (a) d_h= 0 m (b) d_h= 2 m (c) d_h= 4 m.

FIGURE 11. PER versus distance for (a) B = 1 MHz (b) B = 5 MHz (c) B = 10 MHz.

all considered lens systems. Also, consider $d_x = 40$ m, the PER values are $0.2 \times 10^{-7}, 0.4 \times 10^{-7}$, and 0.9×10^{-7} for L2, L1, and L3 lenses, respectively.

In the case of misalignment (i.e., $d_h = 2$ m) (Fig. 10(b)), the three lenses still grant a nearly error-free link in the entire $10-29$ m range. Beyond this range, the L2 lens suffers from worse performances at short distances ($d_x < 10$ m) due to its lower view angle. Also, at long distances $d_x \geq 30$ m, the performance severely degraded and the L2 lens is the best compared to other lenses. For example, consider $d_x = 45$ m, the obtained PER values are $0.4 \times 10^{-7}, 0.9 \times 10^{-7}$, and 3.7×10^{-7} for L2, L1, and L3 lenses, respectively.

In Fig. 10(c), we present the PER versus distance, assuming $d_h = 4$ m. It is observed that error-free communication is achieved in the distance range of $20-30$ m. Outside this range, the performance deteriorates significantly, where the L1 lens gives the best results for short distances ($15-20$ m), and the L2 lens is the best for long distances ($31-50$ m).

In Fig. 11, we present the PER versus distance for different bandwidths. We assume $B = 1$ MHz, 5 MHz, and 10 MHz. It is observed that the error rate increases with increasing values of the bandwidth. This is because the higher the bandwidth, the higher the noise variance. For example, consider the combined lens case and $d_x = 45$ m, the obtained values of PER are $10^{-8}, 0.4 \times 10^{-6}$, and 1.8×10^{-6} for $B = 1$ MHz, $B = 5$ MHz, and $B = 10$ MHz, respectively.

TABLE 2. Lens selection according to incident angle (θ_1).

Incident angle, θ_1	Fresnel Lens	Aspherical Lens	Combined Lens
1.03°-1.69°	✓		
1.70°-13.13°	✓	✓	✓
13.14°-15.43°		✓	✓
15.44°-20.65°		✓	
20.66°-30.11°		✓	✓
30.12°-44.42°			✓

In the following, in order to generalize the lens selection during the car mobility, we analyze the choice of the suitable optical lens according to the angle of incidence of the incoming beam from the two headlamps (i.e. θ_1 and θ_2).

Tables 2 and 3 show the best lens selection for a range of incident angles (i.e., θ_1 and θ_2). Table 2 shows the best lens selection to θ_1. It is observed that for a small angle of incidence, the Fresnel lens may be the better choice. While for a medium and large angle of incidence, the Aspherical lens and the combination lens are the best, respectively. For example, considering $\theta_1 = 1.69°$, the Fresnel lens is the best. Also, considering $\theta_1 = 15.44°$ and $\theta_1 = 44.42°$, the Aspherical lens and the combination lens are, respectively, the best choice.

In Table 3, we select the top lenses based on the incident angle of the rays coming from TX2 (θ_2). It is observed that for small and medium angles of incidence, Fresnel and Aspherical lenses may be the best choice. While for large angles of incidence, the combined lens may be the best. For example,

TABLE 3. Lens selection according to incident angle (θ_2).

Incident angle, θ_2	Fresnel Lens	Aspherical Lens	Combined Lens
[-10.2°− -1.70°]	✓	✓	✓
[-1.69°− 0.18°]	✓		
[0.19°− 2.50°]	✓	✓	✓
[2.51°−3.54°]		✓	✓
[3.55°−5.71°]	✓	✓	✓
[5.72°−6.27°]	✓		
[6.28°−6.79°]	✓	✓	
[6.8°−7.06°]		✓	
[7.07°−8.39°]	✓	✓	
[8.40°−13.40°]		✓	
[13.41°−31.79°]			✓

consider $\theta_2 = -1.69°$, $\theta_2 = 7.06°$, and $\theta_2 = 31.79°$, the most appropriate lenses are respectively Fresnel, Aspherical, and combined lenses.

V. CONCLUSION

In this paper, we have investigated the performance of the V2V-VLC system using an imaging receiver with different kinds of lenses, including Fresnel, Aspherical, and combined lenses. We have conducted a realistic channel modeling approach based on a non-sequential ray-tracing approach, which considers the effect of headlight asymmetrical intensity profiles. The effect of the lens types, receiver types, receiver diameters, and bandwidth was further investigated. A comprehensive performance comparison is then conducted in terms of PER for different kinds of lenses. Our results reveal that with a carefully chosen system and lens parameters, an enhancement of 7 dB in total received power can be achieved. The results also reveal that the Fresnel lens is a good choice for improving performance, especially at long distances.

ACKNOWLEDGMENT

REFERENCES

[1] O. Pribyl, P. Pribyl, M. Lom, and M. Svitek, "Modeling of smart cities based on ITS architecture," *IEEE Intell. Transp. Syst. Mag.*, vol. 11, no. 4, pp. 28–36, Winter 2019.

[2] A. Memedi and F. Dressler, "Vehicular visible light communications: A survey," *IEEE Commun. Surveys Tuts.*, vol. 23, no. 1, pp. 161–181, 1st Quart., 2021.

[3] H. B. Eldeeb, S. M. Sait, and M. Uysal, "Visible light communication for connected vehicles: How to achieve the omnidirectional coverage?" *IEEE Access*, vol. 9, pp. 103885–103905, 2021.

[4] M. Elamassie, M. Karbalayghareh, F. Miramirkhani, R. C. Kizilirmak, and M. Uysal, "Effect of fog and rain on the performance of vehicular visible light communications," in *Proc. IEEE 87th Veh. Technol. Conf.*, Jun. 2018, pp. 1–6.

[5] Y.-H. Kim, W. A. Cahyadi, and Y. H. Chung, "Experimental demonstration of LED-based vehicle to vehicle communication under atmospheric turbulence," in *Proc. Int. Conf. Inf. Commun. Technol. Converg. (ICTC)*, Oct. 2015, pp. 1143–1145.

[6] Y. H. Kim, W. A. Cahyadi, and Y. H. Chung, "Experimental demonstration of VLC-based vehicle-to-vehicle communications under fog conditions," *IEEE Photon. J.*, vol. 7, no. 6, pp. 1–9, Dec. 2015.

[7] C. Tu, W. Liu, and Z. Xu, "Mitigation of strong background radiation with attenuation diversity for vehicular visible light communication," in *Proc. 11th Int. Conf. Wireless Commun. Signal Process. (WCSP)*, Oct. 2019, pp. 1–2.

[8] D.-R. Kim, S.-H. Yang, H.-S. Kim, Y.-H. Son, and S.-K. Han, "Outdoor visible light communication for inter-vehicle communication using controller area network," in *Proc. 4th Int. Conf. Commun. Electron. (ICCE)*, Aug. 2012, pp. 31–34.

[9] C. Tebruegge, Q. Zhang, and F. Dressler, "Optical interference reduction with spatial filtering receiver for vehicular visible light communication," in *Proc. IEEE Intell. Transp. Syst. Conf. (ITSC)*, Oct. 2019, pp. 3055–3061.

[10] H. B. Eldeeb, F. Miramirkhani, and M. Uysal, "A path loss model for vehicle-to-vehicle visible light communications," in *Proc. 15th Int. Conf. Telecommun. (ConTEL)*, Jul. 2019, pp. 1–5.

[11] S.-H. Yu, O. Shih, H.-M. Tsai, N. Wisitpongphan, and R. Roberts, "Smart automotive lighting for vehicle safety," *IEEE Commun. Mag.*, vol. 51, no. 12, pp. 50–59, Dec. 2013.

[12] B. Turan, G. Gurbilek, A. Uyrus, and S. C. Ergen, "Vehicular VLC frequency domain channel sounding and characterization," in *Proc. IEEE Veh. Netw. Conf. (VNC)*, Dec. 2018, pp. 1–8.

[13] Z. Cui, P. Yue, X. Yi, and J. Li, "Research on non-uniform dynamic vehicle-mounted VLC with receiver spatial and angular diversity," in *Proc. IEEE Int. Conf. Commun. (ICC)*, May 2019, pp. 1–7.

[14] H. B. Eldeeb and M. Uysal, "Vehicle-to-vehicle visible light communication: How to select receiver locations for optimal performance?" in *Proc. 11th Int. Conf. Electr. Electron. Eng. (ELECO)*, Nov. 2019, pp. 402–405.

[15] S. Yahia, Y. Meraihi, A. B. Gabis, and A. Ramdane-Cherif, "Multi-directional vehicle-to-vehicle visible light communication with angular diversity technology," in *Proc. 2nd Int. Workshop Hum.-Centric Smart Environ. Health Well-Being (IHSH)*, Feb. 2021, pp. 160–164.

[16] M. Morales-Cespedes, A. A. Quidan, and A. G. Armada, "Experimental evaluation of the reconfigurable photodetector for blind interference alignment in visible light communications," in *Proc. 27th Eur. Signal Process. Conf. (EUSIPCO)*, Sep. 2019, pp. 1–5.

[17] L. Zeng, D. C. O'Brien, H. Le Minh, G. E. Faulkner, K. Lee, D. Jung, Y. Oh, and T. E. Won, "High data rate multiple input multiple output (MIMO) optical wireless communications using white led lighting," *IEEE J. Sel. Areas Commun.*, vol. 27, no. 9, pp. 1654–1662, Dec. 2009.

[18] K. V. S. S. Sushanth and A. Chockalingam, "Performance of imaging receivers using convex lens in indoor MIMO VLC systems," in *Proc. IEEE 87th Veh. Technol. Conf. (VTC Spring)*, Jun. 2018, pp. 1–5.

[19] K. D. Dambul, D. O'Brien, and G. Faulkner, "Indoor optical wireless MIMO system with an imaging receiver," *IEEE Photon. Technol. Lett.*, vol. 23, no. 2, pp. 97–99, Jan. 15, Nov. 11, 2010.

[20] T. Q. Wang, Y. A. Sekercioglu, and J. Armstrong, "Hemispherical lens based imaging receiver for MIMO optical wireless communications," in *Proc. IEEE Globecom Workshops*, Dec. 2012, pp. 1239–1243.

[21] T. Q. Wang, Y. A. Sekercioglu, and J. Armstrong, "Analysis of an optical wireless receiver using a hemispherical lens with application in MIMO visible light communications," *J. Lightw. Technol.*, vol. 31, no. 11, pp. 1744–1754, Apr. 12, 2013.

[22] B. Li, X. Lai, J. Wang, X. Liang, and C. Zhao, "Performance analysis of the imaging receivers using a hemispherical lens for visible light communications," in *Proc. Int. Conf. Wireless Commun. Signal Process.*, Oct. 2013, pp. 1–5.

[23] T. Chen, L. Liu, Z. Zheng, J. Song, K. Wu, and W. Hu, "Fisheye-lens-based space division multiplexing system for visible light communications," *EURASIP J. Wireless Commun. Netw.*, vol. 2015, no. 1, pp. 1–7, Dec. 2015.

[24] T. Chen, L. Liu, B. Tu, Z. Zheng, and W. Hu, "High-spatial-diversity imaging receiver using fisheye lens for indoor MIMO VLCs," *IEEE Photon. Technol. Lett.*, vol. 26, no. 22, pp. 2260–2263, Nov. 15, 2014.

[25] T. Lang, Z. Li, A. Wang, and G. Chen, "Hemispherical lens featured bee-hive structure receiver on vehicular massive MIMO visible light communication system," in *Proc. Int. Conf. Internet Vehicles*. Cham, Switzerland: Springer, 2015, pp. 469–477.

[26] J.-H. Yoo, J.-S. Jang, J. K. Kwon, H.-C. Kim, D.-W. Song, and S.-Y. Jung, "Demonstration of vehicular visible light communication based on LED headlamp," *Int. J. Automot. Technol.*, vol. 17, no. 2, pp. 347–352, Apr. 2016.

[27] B. Aly, M. Elamassie, H. B. Eldeeb, and M. Uysal, "Experimental investigation of lens combinations on the performance of vehicular VLC," in *Proc. 12th Int. Symp. Commun. Syst., Netw. Digit. Signal Process. (CSNDSP)*, Jul. 2020, pp. 1–5.

[28] *Sandrine Auriol*. Accessed: Feb. 28, 2023. [Online]. Available: https://support.zemax.com/hc/en-us/articles/1500005488861-Understanding-the-Detector-Polar

[29] F. Miramirkhani and M. Uysal, "Channel modeling and characterization for visible light communications," *IEEE Photon. J.*, vol. 7, no. 6, pp. 1–16, Dec. 2015.

[30] Z. Nazari Chaleshtori, Z. Ghassemlooy, H. B. Eldeeb, M. Uysal, and S. Zvanovec, "Utilization of an OLED-based VLC system in office, corridor, and semi-open corridor environments," *Sensors*, vol. 20, no. 23, p. 6869, Dec. 2020.

[31] M. Uysal, F. Miramirkhani, O. Narmanlioglu, T. Baykas, and E. Panayirci, "IEEE 802.15.7r1 reference channel models for visible light communications," *IEEE Commun. Mag.*, vol. 55, no. 1, pp. 212–217, Jan. 2017.

[32] A. A. E.-R. El-Fikky, E. M. Eldin, A. H. Fayed, A. A. E. Aziz, M. H. H. Shalaby, and H. M. Aly, "NLoS underwater VLC system performance: Static and dynamic channel modeling," *Appl. Opt.*, vol. 58, no. 30, pp. 8272–8281, 2019.

[33] M. Elamassie, F. Miramirkhani, and M. Uysal, "Performance characterization of underwater visible light communication," *IEEE Trans. Commun.*, vol. 67, no. 1, pp. 543–552, Jan. 2019.

[34] M. Karbalayghareh, F. Miramirkhani, H. B. Eldeeb, R. C. Kizilirmak, S. M. Sait, and M. Uysal, "Channel modelling and performance limits of vehicular visible light communication systems," *IEEE Trans. Veh. Technol.*, vol. 69, no. 7, pp. 6891–6901, May 2020.

[35] F. Erismann, "Design of a plastic aspheric Fresnel lens with a spherical shape," *Opt. Eng.*, vol. 36, no. 4, pp. 988–991, 1997.

[36] R. Kirrbach, M. Faulwasser, and B. Jakob, "Non-rotationally symmetric freeform fresnel-lenses for arbitrary shaped Li-Fi communication channels," in *Proc. Global LIFI Congr. (GLC)*, Jun. 2019, pp. 1–6.

[37] W. J. Smith, *Modern Optical Engineering: The Design of Optical Systems*. New York, NY, USA: McGraw-Hill, 2008.

[38] W. Li, F. Qi, Y. Wang, P. Liu, and Z. Liu, "Refractive aspherical lens for terahertz imaging," *Opt. Commun.*, vol. 433, pp. 14–17, Feb. 2019.

[39] E. Hecht, *Optics*. London, U.K.: Pearson, 2002.

[40] A. Gupta, P. Garg, and N. Sharma, "Hard switching-based hybrid RF/VLC system and its performance evaluation," *Trans. Emerg. Telecommun. Technol.*, vol. 30, no. 2, p. e3515, Feb. 2019.

[41] Z. Wang, Q. Wang, W. Huang, and Z. Xu, *Visible Light Communications: Modulation and Signal Processing*. Hoboken, NJ, USA: Wiley, 2017.

[42] K. Ashraf, S. M. T. Islam, A. S. Hosseini, and A. Ashok, "Motion characterization for vehicular visible light communication," in *Proc. 11th Int. Conf. Commun. Syst. Netw. (COMSNETS)*, Jan. 2019, pp. 759–764.

[43] W. Adrian and R. Jobanputra, "Influence of pavement reflectance on lighting for parking lots," Portland Cement Assoc., Skokie, IL, USA, 2005, pp. 1–25.

[44] *Audi A8*. Accessed: Feb. 28, 2023. [Online]. Available: https://www.audiusa.com/us/web/en/models/a8/a8-sedan/2021/overview.html

[45] *Aspheric Lens*. Accessed: Feb. 28, 2023. [Online]. Available: https://www.edmundoptics.fr/f/condenser-lenses-731b9cef/12868/

[46] *Fresnel Lens*. Accessed: Feb. 28, 2023. [Online]. Available: https://www.edmundoptics.fr/f/aspherically-contoured-fresnel-lenses/12432/

[47] S.-A. Avătămăniţei, C. Beguni, A.-M. Căilean, M. Dimian, and V. Popa, "Evaluation of misalignment effect in vehicle-to-vehicle visible light communications: Experimental demonstration of a 75 meters link," *Sensors*, vol. 21, no. 11, p. 3577, May 2021.

[48] C. Beguni, A.-M. Căilean, S.-A. Avătămăniţei, and M. Dimian, "Analysis and experimental investigation of the light dimming effect on automotive visible light communications performances," *Sensors*, vol. 21, no. 13, p. 4446, Jun. 2021.

SELMA YAHIA received the master's degree in networks and telecommunications from the University of 08 Mai 1945 Guelma, Algeria, in 2019. She is currently pursuing the Ph.D. degree with the LIST Laboratory, University of M'Hamed Bougara Boumerdes, Algeria. Her main research interests include visible light communication, optical wireless communication, optical communication, and optimization.

YASSINE MERAIHI received the Ph.D. degree from the University of M'Hamed Bougara Boumerdes, Algeria, in 2017. He is currently an Associate Professor with the University of M'Hamed Bougara Boumerdes. His research interests include QoS for wireless networks, routing in challenged networks, including WMSNs/VANETs and applications of meta-heuristics to optimization problems.

AMAR RAMDANE-CHERIF received the Ph.D. degree from Pierre and Marie Curie University, Paris, in 1998. Since 2000, he has been a Professor with the University of Versailles Saint-Quentin-en-Yvelines, France. His research interests include software architecture, dynamic architecture, architectural quality attributes, architectural styles, and design patterns.

TU DAC HO (Member, IEEE) received the M.Sc. and Ph.D. degrees in wireless communications from Waseda University, Tokyo, Japan, in 2005 and 2011, respectively. He was an Assistant Professor at Waseda University, from 2011 to 2012, a Postdoctoral Fellow at the Norwegian University of Science and Technology, from 2012 to 2014, and a Senior Researcher at SINTEF, Norway, from 2014 to 2018. He has been an Associate Professor with the Department of Electrical Engineering, UiT The Arctic University of Norway, since 2019. He has participated in and led several scientific projects in Norway and Europe, focusing on communications in the Arctic and the application of unmanned aerial vehicles in autonomous systems. He has published 50 international peer-reviewed publications and book chapters. His research interests include communications and networking, communication protocols, the Internet of Things, wireless sensor networks, cyber-physical systems, network and system optimization, and communications/path planning for unmanned systems. He has served as a Committee Member/Reviewer for many journals from publishers, such as IEEE, Elsevier, Springer, Wiley, IET, IEICE, and AIAA, and flagship conferences, such as GLOBECOM, ICC, and WCNC. He is an Editorial Board Member of *Modern Subsea Engineering and Technology*.

HOSSIEN B. ELDEEB (Senior Member, IEEE) received the B.Sc. degree in electronics and electrical communication engineering from Menoufia University, Egypt, in 2008, the M.Sc. degree in electronics and electrical communication engineering from Cairo University, Egypt, in 2018, and the Ph.D. degree in electrical and electronics engineering from Özyeğin University, Turkey, in 2021. He is currently a Postdoctoral Research Fellow with the KU Center for Cyber-Physical Systems, Khalifa University, Abu Dhabi, UAE. His current research interests include optical and wireless communications, vehicular communications, physical layer security, and intelligent reflecting surfaces.

· · ·